Dynamical coupled-channels effects on pion photoproduction

B. Juliá-Díaz,[1,2] T.-S. H. Lee,[1,3] A. Matsuyama,[1,4] T. Sato,[1,5] and L. C. Smith[1,6]

[1]*Excited Baryon Analysis Center (EBAC), Thomas Jefferson National Accelerator Facility, Newport News, Virginia 22901, USA*

[2]*Departament d'Estructura i Constituents de la Matèria, Universitat de Barcelona, E-08028 Barcelona, Spain*

[3]*Physics Division, Argonne National Laboratory, Argonne, Illinois 60439, USA*

[4]*Department of Physics, Shizuoka University, Shizuoka 422-8529, Japan*

[5]*Department of Physics, Osaka University, Toyonaka, Osaka 560-0043, Japan*

[6]*Department of Physics, University of Virginia, Virginia 22901, USA*

(Received 13 December 2007; revised manuscript received 5 March 2008; published 16 April 2008)

The electromagnetic pion production reactions are investigated within the dynamical coupled-channels model developed by Matsuyama, Sato, and Lee [Phys. Rep. **439**, 193 (2007)]. The meson-baryon channels included in this study are $\gamma N, \pi N, \eta N$, and the $\pi\Delta, \rho N$, and σN resonant components of the $\pi\pi N$ channel. With the hadronic parameters of the model determined in a recent study of πN scattering, we show that the pion photoproduction data up to the second resonance region can be described to a very large extent by only adjusting the bare $\gamma N \to N^*$ helicity amplitudes, while the nonresonant electromagnetic couplings are taken from previous works. It is found that the coupled-channels effects can contribute about 30–40 % of the production cross sections in the Δ (1232) resonance region, and can drastically change the magnitude and shape of the cross sections in the second resonance region. The importance of the loop-integrations in a dynamical approach is also demonstrated. The meson cloud effects as well as the coupled-channels contributions to the $\gamma N \to N^*$ form factors are found to be mainly in the low Q^2 region. Necessary improvements to the model and future developments are discussed.

DOI: 10.1103/PhysRevC.77.045205 PACS number(s): 13.75.Gx, 13.60.Le, 14.20.Gk, 25.30.Rw

I. INTRODUCTION

It is well recognized [1,2] that the data of electromagnetic meson production reactions can be used to reveal the structure of the excited states (N^*) of the nucleon. In this paper, we report on an investigation in this direction within the dynamical coupled-channels model (MSL) presented in Ref. [3] which is being applied at the Excited Baryon Analysis Center (EBAC) of Jefferson Laboratory.

The coupled-channels approach has been used [4–7] in recent years to analyze the meson production reaction data. It is therefore useful to briefly emphasize here the essence of taking a dynamical approach as developed in Ref. [3] and in earlier works [8–19]. Since N^* states are unstable, their structure must couple with the reaction channels in the meson production reactions. To determine correctly the spectrum of N^* states, an analysis of the meson production data must account for the coupled-channels unitary condition. The extracted N^* parameters can be interpreted correctly only when the reaction mechanisms in the short-range region, where we want to map out the N^* structure, have been accounted for. The MSL model meets these two crucial requirements and is therefore suitable for analyzing the world data of meson production reactions induced by pions, photons, and electrons.

Schematically, the MSL model solves the following coupled integral equations in each partial wave:

$$T_{\alpha,\beta}(p_\alpha, p_\beta; E) = V_{\alpha,\beta}(p_\alpha, p_\beta) + \sum_\delta \int p^2 dp V_{\alpha,\delta}(p_\alpha, p) \times G_\delta(p, E) T_{\delta,\beta}(p, p_\beta, E), \quad (1)$$

with

$$V_{\alpha,\beta}(p_\alpha, p_\beta) = v_{\alpha,\beta}(p_\alpha, p_\beta) + \sum_{N^*} \frac{\Gamma^\dagger_{N^*,\alpha}(p_\alpha)\Gamma_{N^*,\beta}(p_\beta)}{E - M^0_{N^*}}, \quad (2)$$

where $\alpha, \beta, \delta = \gamma N, \pi N, \eta N$, and $\pi\pi N$ which has $\pi\Delta, \rho N, \sigma N$ resonant components, $G_\delta(p, E)$ is the propagator of channel δ, $M^0_{N^*}$ is the mass of a bare excited nucleon state N^*, $v_{\alpha,\beta}$ is defined by meson-exchange mechanisms, and the $N^* \to \beta$ vertex interaction $\Gamma_{N^*,\beta}$ is related to the quark-gluon substructure of N^*. If we take the on-shell approximation, Eq. (1) is reduced to the following algebraic form of K-matrix models [4–6,20–22]:

$$T^k_{\alpha,\beta}(p_\alpha, p_\beta, E) = \sum_\delta V_{\alpha,\delta}(p_\alpha, p_\delta) \times \left[\delta_{\delta,\beta} + i\rho(p_\delta) T^k_{\delta,\beta}(p_\delta, p_\beta, E)\right], \quad (3)$$

where $\rho(p_\delta)$ is an appropriate phase space factor. Qualitatively speaking, models that make use of on-shell expressions such as Eq. (3) are used to avoid an explicit treatment of the reaction mechanisms in the short range region where we want to map out the quark-gluon substructure of N^* states. Thus the N^* parameters extracted by using Eq. (1) can be more directly interpreted in terms of the quark-gluon substructure of N^*. From the study [11,19] in the Δ (1232) region, it is reasonable to interpret $\Gamma_{N^*,\beta}$ in terms of hadron structure calculations with effective degrees of freedom, such as the constituent quark model [23] and the model [24] based on Dyson-Schwinger equations. In the near future, one hopes to relate $\Gamma_{N^*,\beta}$ to lattice QCD (LQCD) calculations [25,26]. The possibility of making

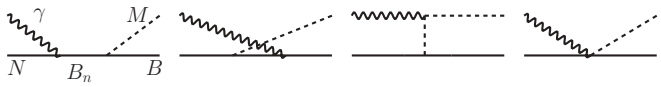

FIG. 1. The nonresonant electromagnetic meson production interaction $v_{MB,\gamma N}$, where $MB = \pi N, \eta N, \pi\Delta, \rho N, \sigma N$. The details are given in Ref. [3].

contact with the current hadron structure calculations, which can be carried out with sufficient accuracy in the foreseeable future, is the main motivation for performing the analysis using a technically much more involved dynamical approach.

To analyze the electromagnetic meson production reactions within the MSL model, it is necessary to first determine the hadronic part of its Hamiltonian. Progress in this direction has been made recently in Ref. [27] (JLMS). The main purpose of this work is to explore the consequence of the parameters determined by JLMS in describing the pion photoproduction reactions. Within the MSL formulation, these hadronic parameters should be consistently used to fix the strong interaction vertices of the nonresonant $\gamma N \to MB$ interaction $v_{MB,\gamma N}$ of Eq. (2). Since the electromagnetic interactions, such as the $\gamma NN, \gamma\pi\rho, \gamma\pi\omega$ vertices of the considered nonresonant mechanisms illustrated in Fig. 1, have been determined in previous works as also given in Ref. [3], the challenge here is to explore whether the pion photoproduction data can be described by only adjusting the bare $\gamma N \to N^*$ vertex $\Gamma_{N^*,\gamma N}$ of Eq. (2).

To proceed, we first note that in the study by JLMS [27] it was found that the fit to πN elastic scattering data is not sufficient for pinning down precisely the hadronic parameters associated with the unstable particle channels $\pi\Delta$, ρN, and σN. These channels have very large effects in the invariant mass $W \geqslant$ about 1.65 GeV region where the two-pion production dominates. It is necessary to include the $\pi N \to \pi\pi N$ data in the fit. This very challenging task is still being pursued at EBAC. For this reason, we will limit our investigation to the $W = 1.1$ GeV–1.65 GeV region which covers the energies of the low-lying nucleon resonances in the so called first and second resonance regions. The resulting model is sufficient for investigating the dynamical coupled-channels effects on the $\gamma N \to \pi N$ cross sections and the $\gamma N \to N^*$ transitions. This is the main focus of this work.

The details of the employed dynamical coupled-channels model have been given in Ref. [3]. In Sec. II we only recall the formulas relevant to the pion photoproduction reactions. The results are presented in Sec. III. Section IV is devoted to discussing the necessary improvements and future developments.

II. FORMULATION

In the helicity-LSJ mixed-representation [3] where the initial γN state is specified by its helicities λ_γ and λ_N and the final MB states by the $(LS)J$ angular momentum variables, the reaction amplitude of $\gamma(\vec{q}) + N(-\vec{q}) \to \pi(\vec{k}) + N(-\vec{k})$ at invariant mass W can be written within the MSL formulation as (suppress the isospin quantum numbers)

$$T^J_{LS_N\pi N,\lambda_\gamma\lambda_N}(k,q,W) = t^J_{LS_N\pi N,\lambda_\gamma\lambda_N}(k,q,W) + t^{R,J}_{LS_N\pi N,\lambda_\gamma\lambda_N}(k,q,W), \quad (4)$$

where $S_N = 1/2$ is the nucleon spin, and the nonresonant amplitude is

$$t^J_{LS_N\pi N,\lambda_\gamma\lambda_N}(k,q,E) = v^J_{LS_N\pi N,\lambda_\gamma\lambda_N}(k,q,E) + \sum_{M'B'}\sum_{L'S'}\int k'^2 dk' t^J_{LS_N\pi N,L'S'M'B'}(k,k',E) \times G_{M'B'}(k',E) v^J_{L'S'M'B',\lambda_\gamma\lambda_N}(k',q,E). \quad (5)$$

In the above equation, the meson-baryon channels included in the sum are $M'B' = \pi N, \eta N, \pi\Delta, \rho N, \sigma N$. The matrix elements $v^J_{LSMB,\lambda_\gamma\lambda_N}(k,q,E)$, which describe the $\gamma N \to M'B'$ transitions, are calculated from the tree diagrams, illustrated in Fig. 1, of a set of phenomenological Lagrangians describing the interactions between $\gamma, \pi, \eta, \rho, \omega, \sigma, N$, and $\Delta(1232)$ fields. The details are given explicitly in Appendix F of Ref. [3]. We will use the hadronic parameters determined by JLMS [27] to evaluate the meson-baryon propagators $G_{M'B'}$ and the $\pi N \to MB$ amplitudes $t^J_{LS_N\pi N,L'S'M'B'}(k,k',E)$, and to also fix the hadronic vertices of the $\gamma N \to MB$ amplitudes $v^J_{LSMB,\lambda_\gamma\lambda_N}(k,q,E)$. As discussed in Sec. I, all of the electromagnetic vertices, such as $\gamma NN, \gamma\pi\pi, \gamma\pi\omega$, in $v^J_{LSMB,\lambda_\gamma\lambda_N}(k,q,E)$ are taken from previous works, as also specified in Ref. [3]. Thus the nonresonant amplitude defined by Eq. (5) is completely fixed in the present investigation. Such a consistent dynamical treatment of strong and electromagnetic reaction mechanisms is highly desirable in using the meson production reactions to study the N^* structure.

The resonant amplitude in Eq. (4) is

$$t^{R,J}_{LS_N\pi N,\lambda_\gamma\lambda_N}(k,q,E) = \sum_{N^*_i,N^*_j}\left[\bar{\Gamma}^J_{N^*_i,LS_N\pi N}(k,W)\right]^* D_{i,j}(W)\bar{\Gamma}^J_{N^*_j,\lambda_\gamma\lambda_N}(q,W), \quad (6)$$

where the dressed vertex functions are defined as

$$\left[\bar{\Gamma}^J_{N^*,LS_N\pi N}(k,W)\right]^* = \left[\Gamma^J_{N^*,LS_N\pi N}(k)\right]^* + \sum_{M'B'}\sum_{L'S'}\int k'^2 dk' t^J_{LS_N\pi N,L'S'M'B'}(k,k',W) \times G_{M'B'}(k',W)\left[\Gamma^J_{N^*,L'S'M'B'}(k')\right]^*, \quad (7)$$

$$\bar{\Gamma}^J_{N^*,\lambda_\gamma\lambda_N}(q,W) = \Gamma^J_{N^*,\lambda_\gamma\lambda_N}(q) + \sum_{M'B'}\sum_{L'S'}\int k'^2 dk' \bar{\Gamma}^J_{N^*,L'S'M'B'}(k',W) G_{M'B'}(k',W) \times v^J_{L'S'M'B',\lambda_\gamma\lambda_N}(k',q). \quad (8)$$

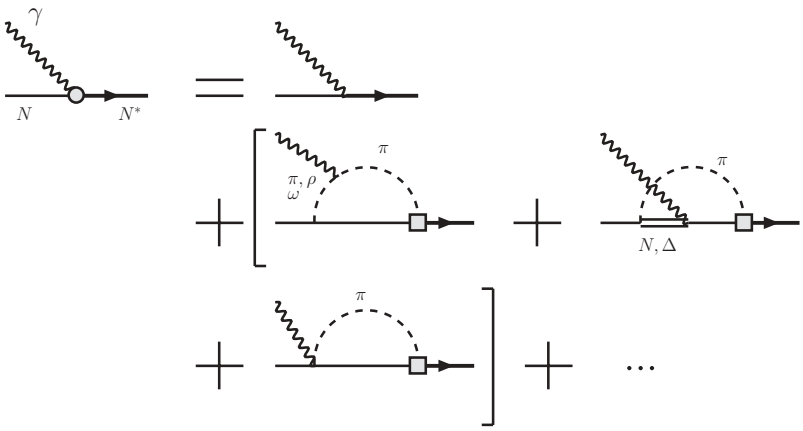

FIG. 2. Graphical illustration of the contribution to the πN intermediate state to the dressed $\gamma N \to N^*$ vertex defined by Eq. (8).

The second term of Eq. (8) is due to the mechanism where the nonresonant electromagnetic meson production takes place before the dressed N^* states are formed. The contribution due to the πN intermediate state is illustrated in Fig. 2. Similar to what was defined in Refs. [11,19], we call this contribution the *meson cloud effect* to define precisely what will be presented in Sec. III.

The N^* propagator in Eq. (6) is defined by

$$[D(W)^{-1}]_{i,j} = \left(W - M^0_{N^*_i}\right)\delta_{i,j} - \bar{\Sigma}_{i,j}(W), \tag{9}$$

where $M^0_{N^*_i}$ is the bare mass of the N^*_i state, and the self-energies are

$$\bar{\Sigma}_{i,j}(W) = \sum_{MB}\sum_{LS}\int dk k^2 \Gamma^J_{N^*_i,LSMB}(k) G_{MB}(k,W) \times \left[\bar{\Gamma}^J_{N^*_j,LSMB}(k,W)\right]^*. \tag{10}$$

Since the dressed vertex $\bar{\Gamma}^J_{N^*,LSMB}(k,W)$ of $N^* \to MB$ in Eqs. (7) and (8) and the bare masses $M^0_{N^*}$ and the mass shifts $\bar{\Sigma}_{i,j}$ in Eq. (9) have been determined by JLMS [27], the only unknown quantities in the resonant amplitude Eq. (6) are the bare $\gamma N \to N^*$ vertex functions $\Gamma^J_{N^*,\lambda_\gamma\lambda_N}(q)$ in Eq. (8). We parametrize these functions as

$$\Gamma^J_{N^*,\lambda_\gamma\lambda_N}(q) = \frac{1}{(2\pi)^{3/2}}\sqrt{\frac{m_N}{E_N(q)}}\frac{1}{\sqrt{2q}}\left[\sqrt{2q_R}A^J_\lambda\right]\delta_{\lambda,(\lambda_\gamma-\lambda_N)}, \tag{11}$$

where q_R is defined by the N^* mass $M_{N^*} = q_R + E_N(q_R)$. For later discussions, we also cast the dressed vertex Eq. (8) into the form of Eq. (11) with a dressed helicity amplitude

$$\bar{A}^J_\lambda(q) = A^J_\lambda + A^{mc,J}_\lambda(q), \tag{12}$$

where $A^{mc,J}_\lambda(q)$ is due to the meson cloud effects defined by the second term of Eq. (8). The dressed helicity amplitude $\bar{A}^J_\lambda$ is related to the partial width of the electromagnetic decay of a N^* resonance defined by

$$\text{[partial decay width]} = \frac{q_R^2}{4\pi}\frac{m_N}{M_{N^*}}\frac{8}{2J+1}\left[\left|\bar{A}^J_{3/2}(q_R)\right|^2 + \left|\bar{A}^J_{1/2}(q_R)\right|^2\right]. \tag{13}$$

Equations (11)–(13) and (8) fix the relation between the bare helicity amplitude A^J_λ of Eq. (8) and the helicity amplitudes $\bar{A}^J_\lambda$ listed by the Particle Data Group (PDG).

III. RESULTS

With the specifications given in Sec. II, our task is to perform χ^2-fits to the available data of $\gamma N \to \pi N$ reactions up to $W = 1.65$ GeV by adjusting the bare helicity amplitudes A^J_λ of the bare N^* states included in the JLMS fit [27] to the πN scattering data. The χ^2-fits are performed by using MINUIT. In this first and second resonance regions, we find that the fits to the data are mainly sensitive to the bare helicity amplitudes listed in Table I. Other bare helicity amplitudes are set to zero in the calculations. The quality of the resulting fit can be seen in Figs. 3, 4, 5 and 6. The solid curves in Figs. 3 and 4 are the calculated differential cross sections $(d\sigma/d\Omega)$ for $\gamma p \to \pi^0 p$ and $\gamma p \to \pi^+ n$, respectively, compared with the corresponding experimental data. Similarly solid curves in Figs. 5 and 6 correspond to the obtained photon asymmetry (Σ_γ) compared to the experimental data for the reactions $\gamma p \to \pi^0 p$ and $\gamma p \to \pi^+ n$, respectively. We see that the model can give an overall good description of the considered data, while significant discrepancies with the data remain.

TABLE I. The bare $\gamma N \to N^*$ helicity amplitudes determined from χ^2-fits to the $\gamma N \to \pi N$ data shown in Figs. 3–6.

Bare N^*	$A_{1/2}[10^{-3}\ \text{GeV}^{-1/2}]$	$A_{3/2}[10^{-3}\ \text{GeV}^{-1/2}]$
$S_{11}-1$	69	–
$S_{11}-2$	−17	–
$S_{31}-1$	188	–
$P_{11}-1$	23	–
$P_{13}-1$	−64	−20
$P_{33}-1$	−78	−132
$D_{13}-1$	47	−72
$D_{15}-1$	47	32
$D_{33}-1$	30	−51
$F_{15}-1$	−97	−63

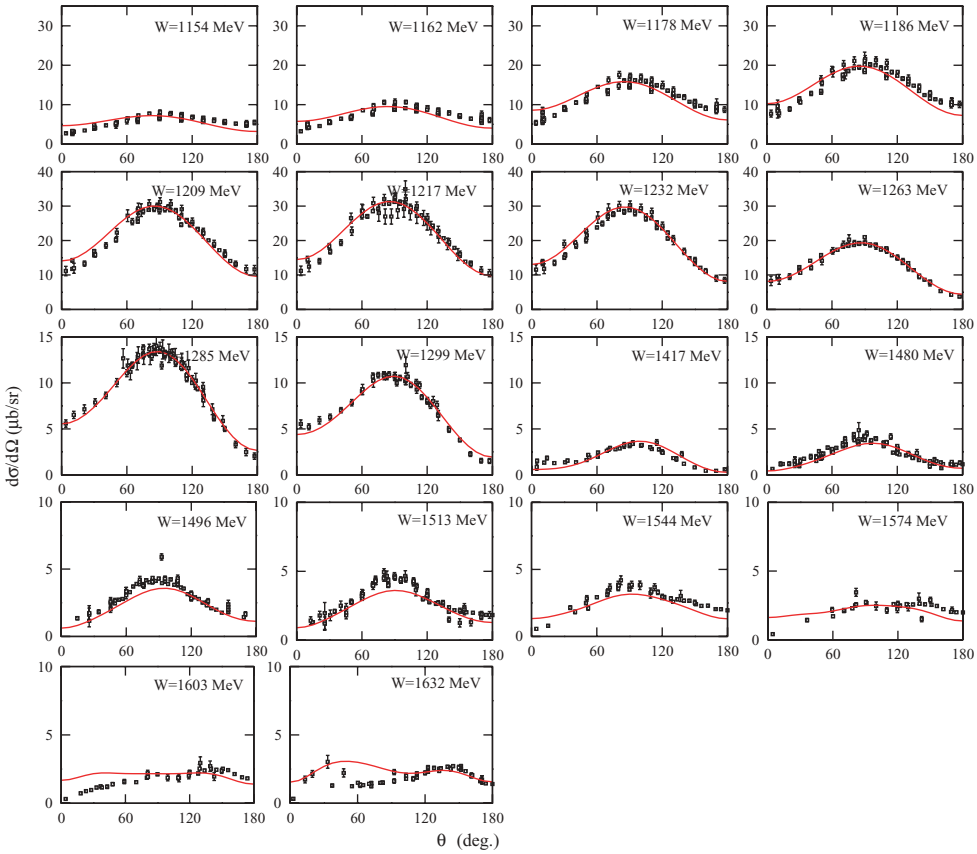

FIG. 3. (Color online) Differential cross section for $\gamma p \to \pi^0 p$ compared to experimental data obtained from Ref. [28].

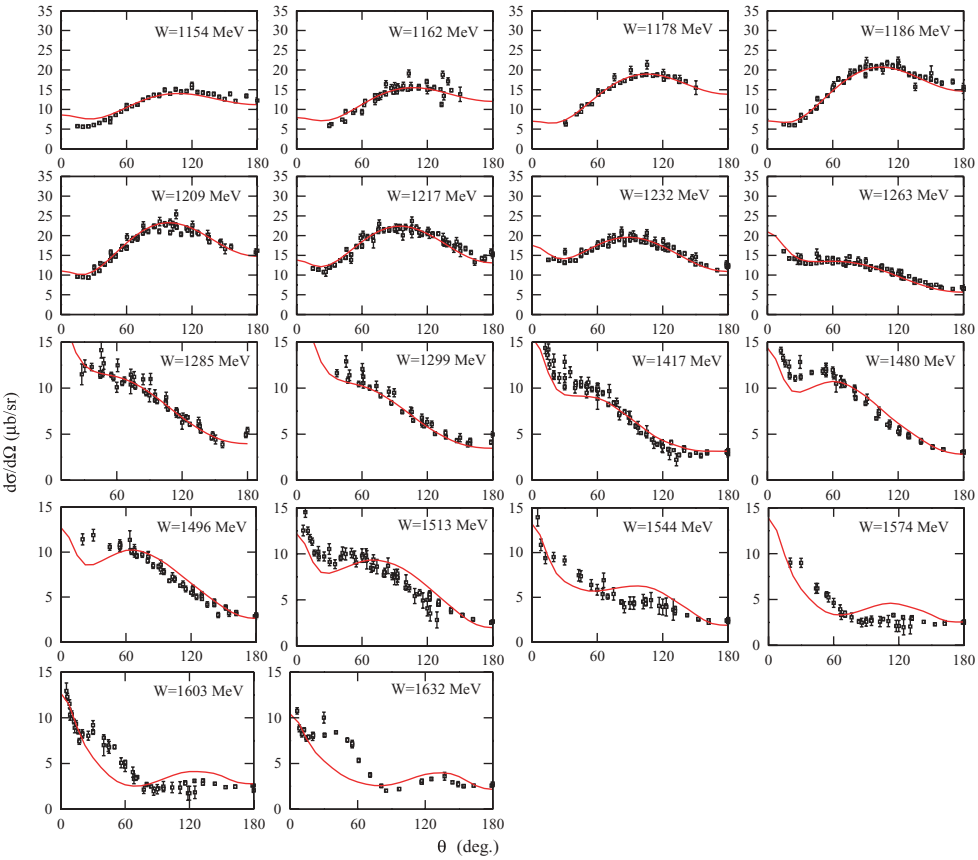

FIG. 4. (Color online) Differential cross section for $\gamma p \to \pi^+ n$ compared to experimental data obtained from Ref. [28].

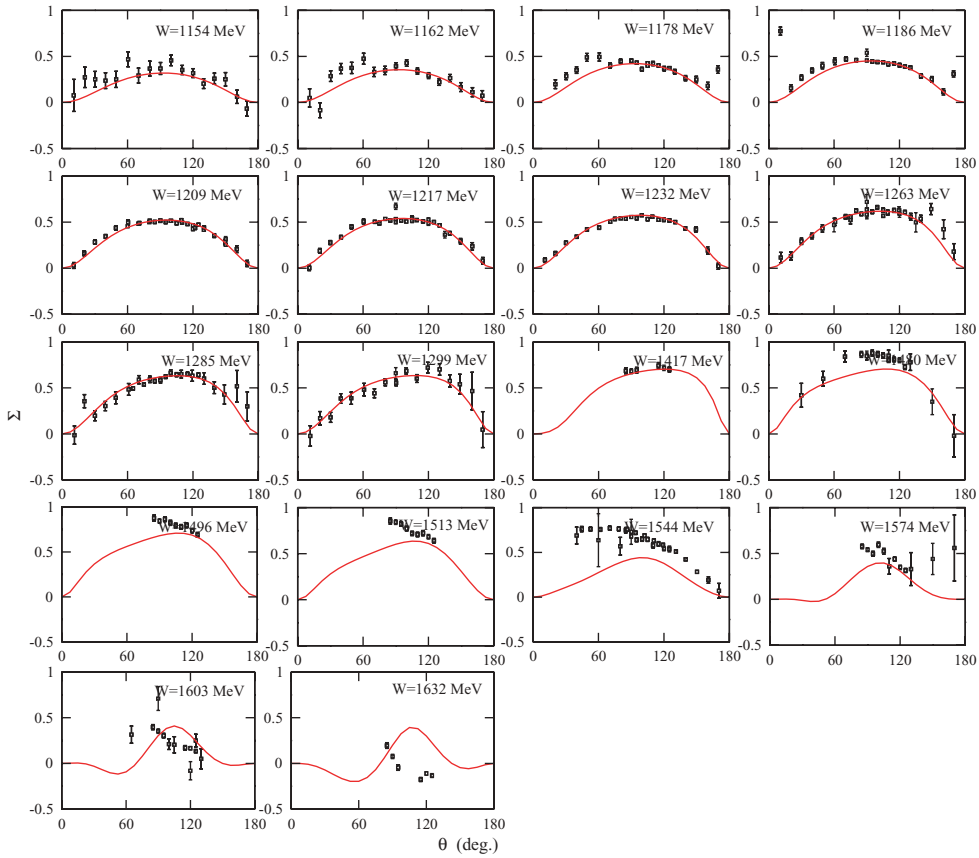

FIG. 5. (Color online) Photon asymmetry, Σ_γ, for $\gamma p \to \pi^0 p$ compared to experimental data obtained from Ref. [28].

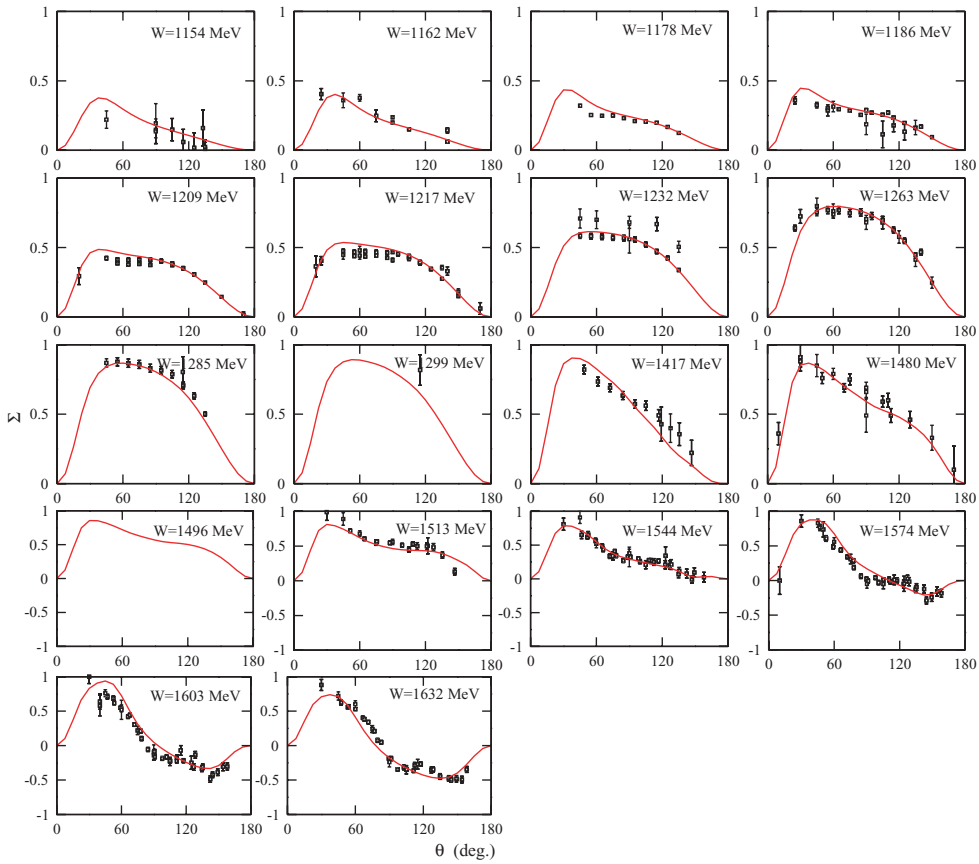

FIG. 6. (Color online) Photon asymmetry, Σ_γ, for $\gamma p \to \pi^+ n$ compared to experimental data obtained from Ref. [28].

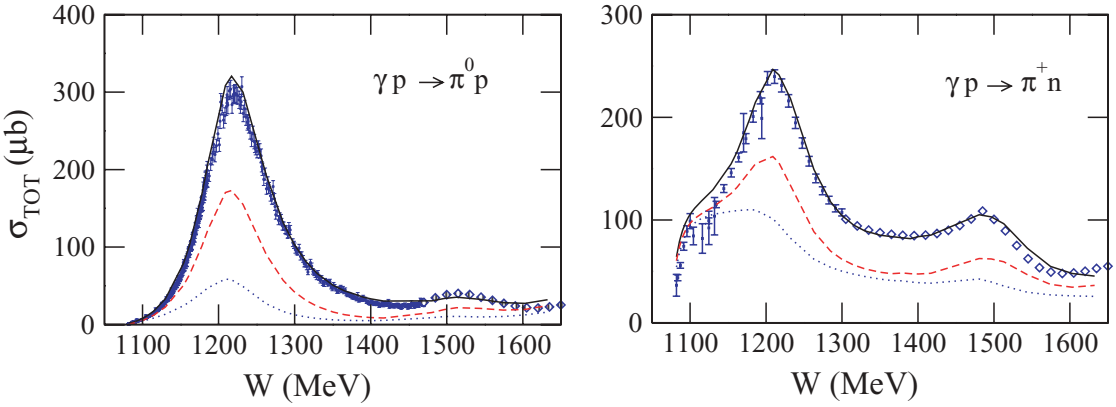

FIG. 7. (Color online) Total cross sections. The dashed curves are obtained from turning off all MB channels except the πN channel in the the loop integrations in the nonresonant amplitude defined by Eq. (5) and the dressed $\gamma N \to N^*$ vertex defined by Eq. (8). The dotted curve is obtained by neglecting the loop-integrations in the πN only calculation. Experimental data obtained using Ref. [28]. The diamonds correspond to the SAID solution [20].

We emphasize here that the determined bare helicity amplitudes listed in Table I are not directly the properties associated with the nucleon resonances. They are simply the properties of the excited nucleon states in the *absence* of coupling to the reaction channels. We need to identify the resonant positions from the partial-wave amplitudes predicted by our model. The dressed helicity amplitudes $\bar{A}^J_\lambda$ calculated at those resonance positions according to Eq. (8) can then be compared to the partial decay widths from the measurements, as seen in Eq. (13). This is being pursued by developing [29] an analytic continuation method to evaluate the reaction amplitudes in the complex energy plane following the dynamical coupled-channels equations of the MSL model [3].

We now turn to investigating the coupled-channels effects. In Fig. 7, we see that the calculated total cross sections (solid curves) are in good agreement with the data. The dashed curves are obtained when the channels ηN, $\pi\Delta$, ρN, and σN are turned off in the loop integrations in the nonresonant amplitude defined by Eq. (5) and the dressed $\gamma N \to N^*$ vertex defined by Eq. (8). Clearly, the coupled-channels effects $\gamma N \to \eta N, \pi\Delta, \rho N, \sigma N \to \pi N$ can change the cross sections by about 30–40% in the $\Delta(1232)$ region and as much as 50% in the $W > 1400$ MeV second resonance region. The corresponding coupled-channels effects on the differential cross sections are shown in Fig. 8. Comparing the solid and dashed curves, we see that the coupled-channels effects can change the magnitudes and shapes of $d\sigma/d\Omega$, in particular at higher energies. We have also found that there exists strong interference between different channels. This is illustrated in the lowest right panel at W = 1544 MeV of Fig. 8. By adding the ρN channel, the predicted differential cross sections are changed from the dashed curve, which does not include any coupled-channels effects, to the dot-dashed curve. When the $\pi\Delta$ channel is also included, the dot-dashed curve is brought up to the dot-dot-dashed curve. The difference between the solid curve (the full coupled-channels result) and the

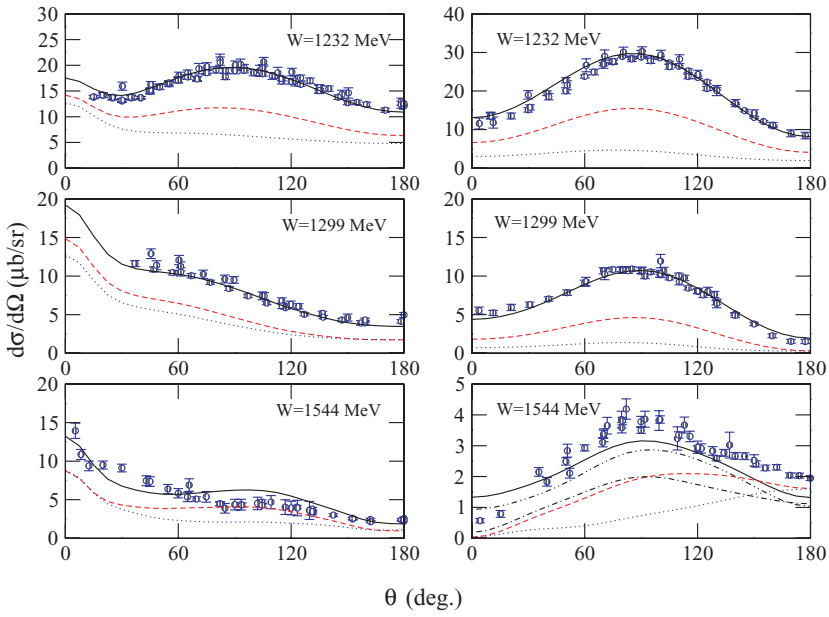

FIG. 8. (Color online) Coupled-channels effects on $d\sigma/d\Omega$ at W = 1.23, 1.30, 1.54 GeV. The dashed curves are obtained from turning off all MB channels except the πN channel in the the loop integrations in the nonresonant amplitude defined by Eq. (5) and the dressed $\gamma N \to N^*$ vertex defined by Eq. (8). The dotted curve is obtained by neglecting the loop integrations in the πN only calculation. Right-hand side: $\gamma p \to \pi^0 p$, left-hand side: $\gamma p \to \pi^+ n$. The lowest right panel at $W = 1544$ MeV includes two additional curves: (a) dot-dashed curve is from including πN and ρN channels, (b) dot-dot-dashed curve is from including πN, ρN, and $\pi\Delta$ channels.

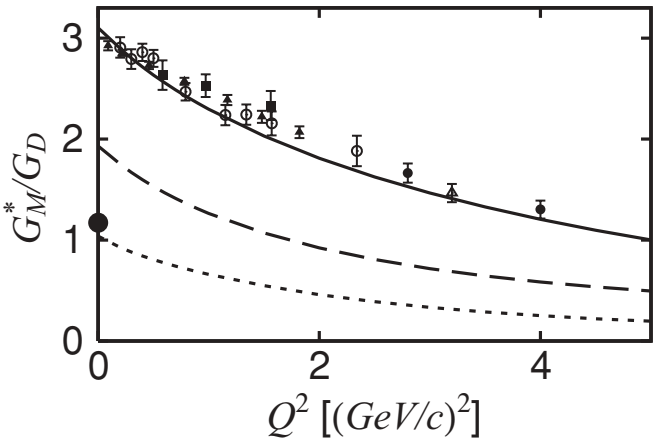

FIG. 9. The predicted Q^2-dependence of meson cloud contributions to the magnetic $M1$ form factor G_M^* defined in Ref. [11] and $G_D(Q^2) = 1/[1 + Q^2/(0.71\,(\mathrm{GeV}/c)^2)]^2$. The dashed curve is the predicted full meson cloud contribution. The dotted curve is obtained after turning off the coupled-channels effects due to $\pi\Delta$ and ρN channels in the loop integrations of Eq. (8). The solid circle at $Q^2 = 0$ is the bare value in the fit. The data are compiled in Ref. [19]. The solid curve along the data is mainly to guide the eyes.

dot-dot-dashed curve is mainly from the constructive interference effects due to adding the σN channel in the calculations. The coupled-channels effect due to ηN is found to be much weaker. Clearly, the results discussed here indicate the need of improving the model by also fitting the $\pi N \to \pi\pi N$ data which can more directly determine the interference between $\pi\Delta$, ρN and σN channels. We will discuss this further in Sec. IV.

As discussed in the introduction, an essential feature of a dynamical approach is to solve integral equations Eqs. (1) and (2) which involve loop integrations. The loop integrations account for the reaction mechanisms at short distances which are not treated explicitly in the technically much simpler K-matrix coupled-channels models [4–6,20–22]. If the loop integrations are neglected in the πN-loop only calculations, we then bring the dashed curves in Figs. 7 and 8 to the dotted curves. Clearly, the loop-integrations effects are very significant, as was also revealed in the coupled-channels calculations [18] of KY photoproduction.

To disentangle the structure of nucleon resonances, it is important to investigate the meson cloud effect on the $\gamma N \to N^*$, as defined by the second term of Eq. (8). It can have contributions from the loop integrations over the πN, ηN, $\pi\Delta$, ρN, σN intermediate states in this calculation. The contribution from the πN loop is that illustrated in Fig. 2. If the electromagnetic form factors associated with the nonresonant interaction $v_{MB,\gamma N}$ are taken from previous works, we can predict the Q^2-dependence of the meson cloud effect term $A_\lambda^{mc,J}$ of Eq. (12).

We first investigate the $\gamma N \to \Delta(1232)$ transition. The resonance position of $\Delta(1232)$ is well defined and reproduced in our calculations as can be seen in the good description of the cross section data near $W = 1232$ MeV in Figs. 3–7. For this isolated resonance, we can follow the procedures detailed in Ref. [11] to calculate the $\gamma N \to \Delta$ (1232) magnetic form factor $G_M^*(Q^2)$ from the imaginary part of the multipole amplitude $M_{1^+}^{I=3/2}$ of $\gamma^* N \to \pi N$ reactions at $W = 1232$ MeV. Our results are shown in Fig. 9. The dashed curve corresponds to the full meson cloud contribution from this calculation. The dotted curve is obtained by keeping only the πN-loop in the calculation. Clearly the difference between the dashed and dotted curves is due to the coupled-channels effects $\gamma N \to \pi\Delta$, $\rho N \to \Delta(1232)$. The solid curve following the data is just to guide the eyes. The difference between the solid curve and the dashed curve provides information about the Q^2-dependence of the bare $\gamma N \to \Delta(1232)$ form factor which can be used as the starting point of our dynamical coupled-channels analysis of pion electroproduction. The solid circle at $Q^2 = 0$ is the corresponding bare value.

For the meson cloud effects on the other $\gamma N \to N^*$ vertex, we calculate the second term of Eq. (8) to get $A_\lambda^{mc,J}$ by using the normalization defined by Eqs. (11) and (12). In Fig. 10, we

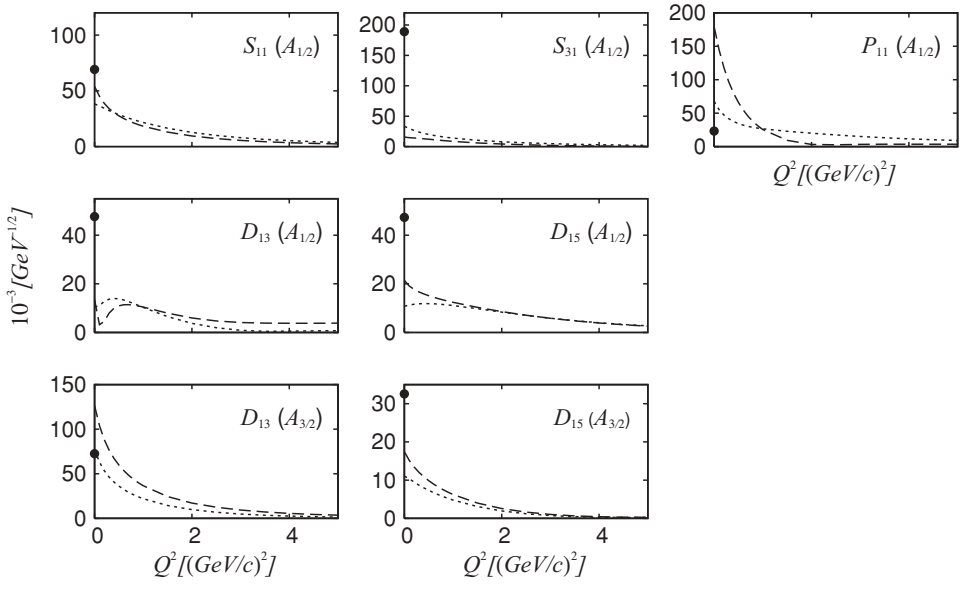

FIG. 10. The predicted Q^2-dependence of meson cloud contributions to the helicity amplitudes $\bar{A}_\lambda^J$. The dotted curves are from keeping only the π-loop in Eq. (8). The black dot corresponds to the absolute value of the bare helicities listed in Table I.

show the predicted magnitudes of $|A_\lambda^{mc,J}|$ evaluated at $W = 1535$ MeV for S_{11}, $W = 1440$ MeV for P_{11}, $W = 1520$ MeV for D_{13}, $W = 1625$ MeV for D_{15}, and $W = 1620$ MeV for S_{31}. The solid dots at $Q^2 = 0$ are the determined bare helicity amplitudes. The dashed curves are from the full meson cloud calculation and the dotted curves are from only keeping the πN loop in Eq. (8). We see that the meson cloud contributions and the coupled-channels effects affect mainly the low Q^2 region.

Here we note that the results presented in Fig. 10 are around the resonance positions listed by the PDG, not from the complex resonance pole positions of our model, which will be determined [29] using an analytical continuation [29]. Thus the results presented here are only for giving some qualitative estimate of the meson cloud effects on $\gamma N \to N^*$ excitation. More accurate predictions will be published in our subsequent analysis [29] of the data of pion electroproduction.

IV. SUMMARY AND FUTURE DEVELOPMENTS

We have applied the dynamical coupled-channels model of Ref. [3] to investigate the pion photoproduction reactions in the first and second nucleon resonance region. With the hadronic parameters of the model determined in a recent study [27] of πN scattering data and the nonresonant electromagnetic couplings taken from the previous works, we show that the available data of differential cross sections and photon asymmetries of $\gamma N \to \pi N$ up to $W = 1.65$ GeV can be described to a very large extent. The only free parameters in the χ^2-fit to the data are the bare $\gamma N \to N^*$ helicity amplitudes. It is found that the coupled-channels effects can have about 30–40 % effects in the Δ (1232) resonance region, and can drastically change the magnitudes and shapes of the cross sections in the second resonance region. We also demonstrate the importance of the loop integrations in a dynamical approach. The meson cloud contributions to the $\gamma N \to N^*$ form factors have been predicted. For all cases, they are mainly in the low Q^2 region. The coupled-channels effects on the meson cloud contributions are also found to be mainly in the low Q^2 region.

The results presented here can be the starting point for analyzing the pion electroproduction data in the first and second resonance region. It will be interesting to see the bare $\gamma N \to \Delta$ (1232) form factor which can be estimated from the differences between the solid and dashed curves in Fig. 9 can be verified in the analysis of the data at $W = 1232$ MeV and $Q^2 \leqslant 6$ (GeV/c)^2. For the data in the second resonance region, our task is to extract the bare helicity amplitudes of $\gamma N \to N^*$ at each Q^2, as was done in this work at the photon point $Q^2 = 0$. Of course the data to be fitted are much more extensive and we need to also determine the longitudinal components of the $\gamma N \to N^*$ vertex. This is being pursued [30] at EBAC.

The most unsatisfactory part of this work is the uncertainties in determining the bare $\gamma N \to N^*$ helicity amplitudes. As seen in Table I, there are 16 helicity amplitudes adjusted in our χ^2-fits to the data. Obviously, it is possible that there could exist other solutions to the minimization problem if more experimental data, in particular polarization data, are included in the fit. Within the MSL formulation [3], these bare parameters are related to hadron structure calculations in the absence of the couplings with reaction channels. A more fruitful approach is to take the helicity amplitudes predicted from such hadron structure calculations as the starting values in our χ^2-fit to avoid unphysical solutions. The resulting parameters could then be used to examine that hadron structure calculation. However more theoretical analysis is needed to know precisely what kind of structure calculations are consistent with the MSL formulation and can be used for this purpose. Since it was found [19] that the extracted bare $\gamma N \to \Delta(1232)$ magnetic $M1$ form factor is fairly consistent with the prediction of constituent quark models, one possibility is to use the relativistic constituent quark model [31].

To improve the agreement with the data, one necessary next step is to improve the hadronic parameters of the model. These parameters, fixed at the values from the fit to πN scattering data, must be improved by performing a combined analysis of both the πN elastic scattering and $\pi N \to \pi\pi N$ data. We expect that the parameters associated with the unstable particle channels, $\pi\Delta$, ρN, and σN, will be refined most significantly. Thus the predicted coupled-channels effects on $\gamma N \to \pi N$ cross sections, as shown in Fig. 8 will be changed such that the fits to the data shown in Figs. 3–6, in particular in the high W region, can be improved. Furthermore, this is also needed to extend our investigation to the third resonance region where the two pion production dominates and the coupled-channels effects through these unstable particle channels are expected to be very large.

Finally, we would like to address the questions concerning how the results from JLMS and this investigation can be used to extract the positions and widths of nucleon resonances. The resonances positions are the poles of the reaction amplitudes in the complex energy plane. The residues of these poles can then be related to the partial decay widths. If these poles are identical to the zeros of the N^* propagator $D_{i,j}(E)$ Eq. (9), we then have the most desirable interpretation that the nucleon resonance is due to the coupling of the bare N^* with the reaction channels. The dressed vertex functions $\Gamma_{N^*,\gamma N}$, defined by Eq. (8), evaluated at these poles can be used to predict the dressed helicity amplitudes $\bar{A}_\lambda$ for calculating the partial decay widths using Eq. (13). On the other hand, the poles could be from the nonresonant amplitude such as the term $t^J_{LS_N\pi N,\lambda_\gamma\lambda_N}$ of Eq. (4). Then the identified resonances have nothing to do with the bare N^* states and are simply due to the attractive meson-baryon interactions. Extraction of this resonance information requires developing numerical methods for solving the dynamical coupled-channels equations on the complex energy plane. Our effort in this direction will be published elsewhere [29].

ACKNOWLEDGMENTS

We would like to thank Dick Arndt for useful discussions. We thank Mark W. Paris for pointing out a coding error in the calculation of the γN-ρN matrix element. B.J-D. acknowledges the support of the Japanese Society for the Promotion of

Science (JSPS), grant no. PE 07021. B.J-D. thanks the nuclear theory group at Osaka University for their warm hospitality. This work is supported by the US Department of Energy, Office of Nuclear Physics Division, under contract No. DE-AC02-06CH11357, and Contract No. DE-AC05-060R23177 under which Jefferson Science Associates operates Jefferson Lab, and by the Japan Society for the Promotion of Science, Grant-in-Aid for Scientific Research (c) 15540275. This work is also partially supported by Grant No. FIS2005-03142 from MEC (Spain) and FEDER and European Hadron Physics Project RII3-CT-2004-506078. The computations were performed at NERSC (LBNL) and Barcelona Supercomputing Center (BSC/CNS) (Spain). The authors thankfully acknowledge the computer resources, technical expertise and assistance provided by the Barcelona Supercomputing Center - Centro Nacional de Supercomputacion (Spain).

[1] V. Burkert and T.-S. H. Lee, Int. J. Mod. Phys. E **13**, 1035 (2004).
[2] T.-S. H. Lee and L. C. Smith, J. Phys. G **34**, S83 (2007).
[3] A. Matsuyama, T. Sato, and T.-S. H. Lee, Phys. Rep. **439**, 193 (2007).
[4] T. Feuster and U. Mosel, Phys. Rev. C **58**, 457 (1998); **59**, 460 (1999); V. Shklyar, H. Lenske, U. Mosel, and G. Penner, *ibid*. **71**, 055206 (2005).
[5] A. Usov and O. Scholten, Phys. Rev. C **72**, 025205 (2005).
[6] A. V. Sarantsev, V. A. Nikonov, A. V. Anisovich, E. Klempt, and U. Thoma, Eur. Phys. J. A **25**, 441 (2005).
[7] G. Y. Chen, S. S. Kamalov, S. N. Yang, D. Drechsel, and L. Tiator, Phys. Rev. C **76**, 035206 (2007) [arXiv:nucl-th/0703096].
[8] S. N. Yang, J. Phys. G **11**, L205 (1985).
[9] S. Nozawa, B. Blankleider, and T.-S. H. Lee, Nucl. Phys. **A513**, 459 (1990).
[10] F. Gross and Y. Surya, Phys. Rev. C **47**, 703 (1993).
[11] T. Sato and T.-S. H. Lee, Phys. Rev. C **54**, 2660 (1996); **63**, 055201 (2001).
[12] S. S. Kamalov and S. N. Yang, Phys. Rev. Lett. **83**, 4494 (1999).
[13] O. Krehl, C. Hanhart, S. Krewald, and J. Speth, Phys. Rev. C **60**, 055206 (1999); **62**, 025207 (2000).
[14] A. D. Lahiff and I. R. Afnan, Phys. Rev. C **66**, 044001 (2002).
[15] M. G. Fuda and H. Alharbi, Phys. Rev. C **68**, 064002 (2003).
[16] V. Pascalutsa and J. A. Tjon, Phys. Rev. C **61**, 054003 (2000).
[17] W. T. Chiang, F. Tabakin, T.-S. H. Lee, and B. Saghai, Phys. Lett. **B517**, 101 (2001).
[18] B. Julia-Diaz, B. Saghai, T.-S. H. Lee, and F. Tabakin, Phys. Rev. C **73**, 055204 (2006).
[19] B. Julia-Diaz, T.-S. H Lee, T. Sato, and L. C. Smith, Phys. Rev. C **75**, 015205 (2007).
[20] R. A. Arndt, I. I. Strakovsky, and R. L. Workman, Phys. Rev. C **53**, 430 (1996); Int. J. Mod. Phys. A **18**, 449 (2003); Phys. Rev. C **66**, 055213 (2002).
[21] D. Drechsel, O. Hanstein, S. S. Kamalov, and L. Tiator, Nucl. Phys. **A645**, 145 (1999); S. S. Kamalov, S. N. Yang, D. Drechsel, O. Hanstein, and L. Tiator, Phys. Rev. C **64**, 032201(R) (2001).
[22] I. G. Aznauryan, Phys. Rev. C **68**, 065204 (2003).
[23] S. Capstick and W. Roberts, Phys. Rev. D **49**, 4570 (1994).
[24] P. Maris and C. D. Roberts, Int. J. Mod. Phys. E **12**, 297 (2003).
[25] C. Alexandrou, G. Koutsou, T. Leontiou, J. W. Negele, and A. Tsapalis, Phys. Rev. D **76**, 094511 (2007).
[26] D. Richards, arXiv:0711.2048 [nucl-th].
[27] B. Julia-Diaz, T.-S. H. Lee, A. Matsuyama, and T. Sato, Phys. Rev. C **76**, 065201 (2007).
[28] CNS Data Analysis Center, George Washington University, http://gwdac.phys.gwu.edu.
[29] N. Suzuki, T. Sato, and T.-S. H. Lee, Proceedings of MENU2007 (to be published).
[30] B. Julia-Diaz, T.-S. H. Lee, A. Matsuyama, T. Sato, and L. C. Smith (in preparation).
[31] B. Julia-Diaz, D. O. Riska, and F. Coester, Phys. Rev. C **69**, 035212 (2004); **75**, 069902(E) (2007).